PREPARATION AND CHARACTERIZATION OF METAL SULPHIDE NANOPARTICLES FOR PHOTOCATALYTIC APPLICATIONS

Dr. Anil Kumar

Department of Chemistry ,D.A.V(PG)College Dehradun
anilpaldav@gmail.com

ABSTRACT

Metal sulphide nanoparticles have become an area of intense study as semiconductors for photocatalytic applications due to the ability to control their electronic structure, their nanoscale surface chemistry, and the prospect of pollutant degradation. In this study, the preparation and characterization of zinc sulphide nanoparticles prepared by controlled aqueous precipitation method and their photocatalytic performance are investigated. Scanning electron microscopy, transmission electron microscopy and energy-dispersive X-ray spectroscopy were used to investigate the surface morphology of the samples, their particle dimensions, and their elemental composition, respectively. X-ray diffraction was used to examine the structural properties of the samples. The optical and chemical properties were determined by ultraviolet–visible (UV-Vis) spectroscope and Fourier-transform infrared (FT-IR) spectroscope. The synthesized nanoparticles of zinc sulphide had a nanocrystalline cubic zinc-blende structure, near stoichiometric zinc to sulphur ratio and had a wide optical band gap of around 3.82eV. The photocatalytic activity was tested under controlled irradiation against a water pollutant model, the methylene blue. Results of the analyses showed that the dye degradation was progressive with irradiation time and followed apparent pseudo-first order kinetic behaviour. The results have shown that the overall performance of photocatalytic reactions is synergistically affected by the crystallinity, size, surface properties and optical characteristics. While pristine ZnS exhibits some activity, the wide band-gap absorption, charge recombination, aggregation and photocorrosion require heterojunction, doping, and surface modification to achieve better visible-light photocatalytic activity, as well as long-term environmental remediation applications.

KEYWORDS

The Zinc Sulphide nanoparticles are synthesized by the photocatalysis method in the presence of methylene blue degradation agent.The Zinc Sulphide nanoparticles are synthesized by the photocatalysis method using the methylene blue degradation agent as an agent.

Doi:10.48047/ijiee.2017.7.1.10

1. INTRODUCTION

1.1 Background and Significance of Nanomaterials

The ability to change the surface, optical, electronic or catalytic properties of matter by decreasing the size to nanometres has made nanomaterials a focus in advanced materials research. Nanoparticles have a higher percentage of surface atoms, shorter charge transport distances and size dependent electronic structures compared to bulk solids. These properties can enhance the chemical reactivity, offer the possibility of regulation of light absorption, charge separation, and interfacial reactions. For photocatalytic applications, nanostructuring is useful since smaller particles have more active sites and reduce the diffusion length of the carriers generated by the photocatalytic reaction to the surface. Semiconductor dimensions could also be of the same order as characteristic excitonic length scales, which may alter the energy of the conduction and valence bands due to quantum confinement (Cargnello & Diroll, 2014). Thus, the nanoscale engineering allows the researchers to fine-tune the size, shape, crystallinity and surface chemistry of the particles according to their target applications. This tunability has promoted the use of semiconductor nanoparticles for environmental remediation, solar energy harvesting, sensing, and catalytic applications that rely on the efficient interaction between light and matter.

1.2 Metal Sulphide Nanoparticles and Their Unique Properties

Metal sulphide nanoparticles are a type of semiconductor nanoparticles because after photoinduced redox reaction the electronic structures in sulfur based lattices can be suitable. Representative systems are CdS, ZnS, CuS, NiS, CoS, SnS2, MoS2 and binary or multicomponent chalcogenides. The photocatalytic relevance of their properties includes the tunability of their band gap, their ability to respond to visible light, the high surface area and a composition dependent charge transport behaviour. Semiconductor sulphides have filled valence bands and empty conduction bands, allowing photoexcitation of the semiconductor when the energy of the photons is equal to or greater than the semiconductor's band gap (Wu et al., 2015). CdS is also notable for its band alignment that allows visible light driven reduction chemistry, but may be limited by instability under illumination and/or prolonged use. The morphology, particle size, exposed facets, crystallinity, defects and the architecture of the interfaces all have a significant effect on the performance of the material. Hence, the ability to prepare and characterize the nanostructure in a controlled way is crucial for making correlation between the nanoscale structure and the optical response and carrier dynamics, surface reactivity, and photocatalytic efficiency in metal sulphide systems.

1.3 Environment applications

The photocatalytic way to increase oxidation and reduction reactions on semiconductor surfaces has been of interest for environmental cleanup and renewable energy conversion, and is a light driven process. If a semiconductor absorbs photons with enough energy, its electrons are excited to the conduction band leaving behind positive holes. These charge carriers may approach the surface sites and participate in reduction or oxidation reactions and the high recombination rate reduces useful quantum efficiency (Qu & Duan, 2013). Not only can the

Doi:10.48047/ijiee.2017.7.1.10

photogenerated holes and electrons produce highly reactive pollutant degradation products such as hydroxyl and superoxide radicals in aqueous pollutant treatment, but they can also catalyze pollutants to break down or mineralize (Ajmal et al., 2014). This phenomenon makes heterogeneous photocatalysis interesting for the treatment of dyes and other persistent pollutants, which could be hard to be removed by other biological or physical degradation methods. The study of photocatalytic materials is also explored for hydrogen generation and production of solar fuels, establishing connections between pollution control and sustainable energy technologies (Cargnello & Diroll, 2014).

1.4 Problems and challenges

Although the potential for metal sulphide photocatalysts is great, they have restrictions that limit their use in practice. The photogenerated electrons and holes can be trapped and recombine before reaching active surface sites, resulting in generation of hot electrons and holes and decreasing of photocatalytic activity (Qu & Duan, 2013). Some sulphides also photocorrode as holes produced under irradiation can oxidize the sulphide lattices. CdS is famous for its photoinstability, which affects its durability and may lead to the discharge of undesirable Cd species during the operation (Wu et al., 2014). Nanoparticles in solution can aggregate, reducing the available surface area and changing the light absorbing properties. Therefore, practical systems need to be able to harvest the light, separate the charges, be structurally stable, inherently low in toxicity, recoverable, reproducible in synthesis and active.

1.5 The aim and the objectives of the research

In this study, the production of metal sulphide nanoparticles and their optical, structural and morphological properties were examined and their effects on photocatalytic activity were studied. It aims at the synthesis of the sulphide material under controlled conditions, confirmation of the crystal phase and crystallinity, examination of the particle morphology, particle size and elemental composition, identification of the chemical features on the surface, assessment of optical absorption and estimation of the band gap energy, and determination of the degradation performance of the material in photocatalytic degradation of a model pollutant. The study aims to assess the degradation kinetics and to correlate activity with physico-chemical properties. The investigation is planned to provide a structure property activity relationship of the prepared photocatalyst by combining the preparation, characterization, and performance testing.

1.6 Novelty and Contribution of the Study

The study does not separate synthesis and performance, but adds to the evaluation of preparation conditions, nanoscale characteristics, photocatalytic response. It is novel because it brought together the crystal, morphological, elemental and optical features that can be determined with this catalyst with the degradation efficiency and kinetic behaviour giving an idea of the features which govern the practical photocatalytic performance of metal sulphide nanoparticles.

Doi:10.48047/ijiee.2017.7.1.10

2. THE LITERATURE REVIEW AND THEORETICAL BACKGROUNDS

2.1 Fundamentals of Semiconductor Photocatalysis

The principle of semiconductor photocatalysis was first proposed by Fujishima and Honda (1972) who exposed a titanium dioxide electrode to sunlight and observed that the electrode could split water into oxygen and hydrogen. They found that absorbed photons can move electrons from the valence band to the conduction band, resulting in the presence of positive holes that can take part in oxidation reactions. The concept of using electrodes for photocatalytic reactions was later expanded to dispersed semiconductor particles by following research. Qu and Duan (2013) pointed out that the real efficiency of photocatalytic reactions relies on a number of interconnected processes: photon absorption, production of electron–hole pairs, migration of charge carriers, interfacial redox reactions, and recombination.

2.2 Properties of Metal Sulphide Photocatalysts

Hisatomi et al. (2014) have reviewed the semiconductor materials used in solar photocatalysts and pointed out that many sulphide semiconductors have narrower band gaps than oxide photocatalysts, which enable them to absorb longer wavelength light. This property is advantageous for visible-light applications, but these applications are still restricted based on the photochemical stability, surface chemistry, carrier mobility, and band alignment of the metal sulphides. These benefits were shown by Li et al. (2015) in a heterostructure of mesoporous ZnS and Zn1−xCdxS/CdS, in which the mediating interface of sulphide facilitated charge transfer and significantly improved the stability and hydrogen-evolution activity. Metal sulphides like CdS, ZnS, CuS, SnS2, MoS2, and other related compounds can thus be tailored in electronic structure and crystal morphology. They can have a very short carrier-diffusion distance and a large surface reaction area in their nanoscale structures. However, sulphide photocatalysts can be prone to photocorrosion, oxidation of lattice sulfur, particle aggregation or fast electron–hole recombination. Therefore, rational control of particle dimensions, defects, crystallinity, exposed surfaces, and heterointerfaces is crucial to ensure efficient and durable photocatalytic activity.

2.3The preparation methods of metal sulphide nanoparticles are described here.

Dunne et al. (2014) have shown that continuous hydrothermal synthesis can be used as a scalable method for the production of a range of nanomaterials such as ZnS, CdS, PbS, CuS, iron sulphide and Bi2S3 with a controllable size and shape. The results they presented showed the impact of the reaction temperature and the nucleation–growth balance on the dimensions and morphology of the nanoparticles. Another method of preparation of metal sulphide nanoparticles is the chemical precipitation or co-precipitation, reaction of soluble metal ions with the sulphide source at controlled pH, concentration and temperature in order to produce low solubility products. Crystallization is favored by solvothermal and hydrothermal methods performed in closed vessels, which can lead to the formation of well-defined morphologies,

Doi:10.48047/ijiee.2017.7.1.10

while microwave-assisted and sonochemical methods increase the nucleation rate by the fast heating process and/or by the generation of acoustic cavitation. Homogeneous precursor mixing and porous products are achievable by sol–gel routes, and biological/Green synthesis aims to substitute dangerous reagents with plant extracts, microorganisms or benign stabilizers. Precursor chemistry too is a significant design variable, as precursor conversion kinetics had proven to play a key role in the nucleation and growth of Cd chalcogenide nanocrystals (García-Rodríguez et al. 2013). Therefore, crystal characteristics such as crystal phase, crystal size, crystal shape, crystal purity, production scalability, reaction time, energy consumption and environmental compatibility and reproducibility between production batches should be taken into consideration when selecting synthesis methods.

2.4 Properties of Metal Sulphide Nanoparticles

Xiong and Zhao (2014) used X-ray diffraction, nitrogen adsorption, electron microscopy and ultraviolet–visible diffuse-reflectance spectroscopy to characterize CdS-containing photocatalytic composites, demonstrating the complementary nature of the information needed to correlate the structure of these materials with their activity. XRD can be used for the identification of crystalline phases and can complement crystallite-size estimation, while SEM can provide information on the surface morphology and aggregation. TEM offers dimension, shape and interfaces. Elemental composition is verified by EDX or EDS. FTIR can identify surface functional groups and chemical bonding environments, while UV–Vis absorption or diffuse-reflectance measurements can provide optical response and give an estimation of the band-gap.

2.5 The photocatalytic applications

Amino-acid-stabilized CdS quantum dots were prepared by Zhang et al. (2015) that absorbed the visible light and photocatalytically degraded rhodamine B and methylene blue, in which the hydroxyl radicals were suggested to play a role in the reaction pathway. They were able to show over repeated cycles the ability of their catalyst to remain active, as well as being stable. To maximize light absorption, charge separation and electron transport, Pawar et. al. (2014) suggested that CdS be coupled with graphitic carbon nitride and reduced graphene oxide which led to improved degradation under visible light. Likewise, Sun et al. (2014) showed that the composite of g-C3N4/Zn0.25Cd0.75S could degrade dyes and reduce Cr(VI). Overall, the results of these studies demonstrate that the composition and interfacial engineering can significantly enhance sulphide photocatalysis.

2.6 Research Gap

Qu and Duan (2013) pointed out that simultaneous light harvesting, efficient charge separation, catalytic activity, stability, and cost are a challenge for photocatalysts. Photocorrosion, aggregation and toxic-metal issues need to be improved for metal sulphides. Therefore, it is still required to correlate the synthesis conditions, the physicochemical characteristics, degradation kinetic, and durability of useful sulphide nanophotocatalysts.

Doi:10.48047/ijiee.2017.7.1.10

3. MATERIALS AND METHODS

3.1 Materials and Chemicals

A typical metal sulphide photocatalyst, zinc sulphide (ZnS), was chosen. Zinc acetate dihydrate, sodium sulphide nonahydrate, sodium hydroxide, ethanol, and methylene blue were used as analytical grade reagents. Deionized water was used as the main solvent for all the synthesis and photocatalytic experiments. The zinc acetate served as a source of Zn2+ ions and sodium sulphide as a source of S2− ions for controlled precipitation. Washing was done with ethanol to help with the removal of residual organic and ionic species. If pH adjustment was necessary, it was done with the use of sodium hydroxide. The model aqueous pollutant chosen was methylene blue due to the ability for its concentration to be monitored spectrophotometrically during experiments of photocatalytic degradation.

3.2 Preparation/Synthesis of Metal Sulphide Nanoparticles

The ZnS nanoparticles were synthesized using a controlled aqueous precipitation method similar to those used for the preparation of metal sulphide nanomaterials (Dunne et al., 2014; Lee et al., 2013). The zinc acetate solution was normally 0.1 M and made in 100 mL of deionized water, stirred and dissolved magnetically. 0.1 M sodium sulphide solution was prepared separately in 100 mL of deionized water. To control the uncontrolled growth of particles, the sulphide solution was slowly added to the zinc precursor with strong stirring at room temperature to guarantee homogeneous nucleation. The molar ratio of Zn2+/S2- was kept at 1:1 to ensure the formation of the products in a stoichiometric ratio of ZnS.

When adding, the suspension was stirred for 2 h continuously. If pH is not maintained in a narrow range (neutral to slightly alkaline) then precursor speciation and reaction environment may affect the nucleation, growth, aggregation, and final particle morphology (Dunne et al., 2014). Sulphide precipitation was considered to be indicated by the formation of whitish precipitate of ZnS. The suspension was aged for 12 h at room temperature after the addition of reagents to allow precipitation to be completed and structural growth to take place.

The general form of the precipitation reaction was written as $Zn^{2+} + S^{2-} \rightarrow ZnS(s)$. The old suspension was centrifuged, the solid was repeatedly washed and then dried. A precipitation method was chosen because it allows for easy control of the concentration of precursors in the solution, the rate at which they can be added, the acidity of the reaction, the temperature of the reaction, and the aging time of the reaction without the need for complicated instrumentation. For photocatalytic materials obtained by solution processes, the morphological, compositional and interfacial structure has been found to have a significant influence on optical absorption and photocatalytic activity (Lee et al., 2013). For all experiments, the same concentrations of reagents and processing conditions were used to ensure reproducibility and the ability to compare the results of characterization with those of photocatalytic experiments. The process gave a uniform standard to investigate the effect that the structure of the nanoscale ZnS has on the subsequent removal of pollutants by light.

Doi:10.48047/ijiee.2017.7.1.10

3.3 The purification, drying, and sample preparation

The precipitated ZnS was centrifuged at about 6000 revolutions per minute (rpm) for 10 min to separate it from the mother liquor. It is washed 3 times with deionized water to remove soluble ionic residues and twice with ethanol to reduce weakly bound impurities and to aid drying. The suspension was re-dispersed after each washing and re-centrifuged. The washed precipitate was dried for 12 h at 70 °C, then was ground gently with an agate mortar and pestle and stored in airtight glass containers. Powder used for the characterization and the photocatalytic tests was from the same batch to minimise sample-to-sample variation and to ensure consistency.

3.4 Structural Characterization: XRD

The crystalline phase, structural purity and average crystallite size of the synthesized ZnS was determined by powder X-ray diffraction technique. The diffraction patterns were taken with Cu Kα radiation in an appropriate 2θ region that includes the characteristic ZnS reflections. The phase identification was made by matching the positions of the peaks obtained from the experiment with the standard crystallographic reference data. Average crystallite dimensions were estimated by peak broadening using the Scherrer relationship (Scherrer 1918): $D = K\lambda/(\beta\cos\theta)$, where D is the average crystallite dimension, K is the shape factor, λ is the X-ray wavelength, β is the FWHM and θ is the Bragg angle for each sample being analyzed.

3.5 Morphological and Elemental Characterization: SEM/TEM/EDX.

The surface morphology and particle organization was investigated using scanning electron microscopy and higher resolution data on particle dimensions, shape, aggregation and nanostructure was obtained by transmission electron microscopy. For SEM samples were mounted on conductive holders and were coated if required to prevent charging. The powder was briefly ultrasonically dispersed in ethanol, placed on a carbon-coated copper grid and dried prior to TEM imaging. In order to confirm the presence and relative distribution of zinc and sulfur, energy-dispersive X-ray spectroscopy was used in conjunction with the electron microscopy. The method is a morphological and elemental characterization that is well established for characterization of ZnS photocatalysts and other nanostructured sulphides (Lee et al., 2013; Xiong & Zhao, 2014). To avoid imaging bias, representative micrographs were obtained throughout the regions.

3.6 Optical and chemical characterization of the compounds, including UV–Vis and FTIR analyses and related techniques

The optical absorption was studied in the ultraviolet and visible regions by UV–visible spectroscopy. Spectra were used to identify the absorption edge and the transformed absorption term was plotted against the photon energy to estimate the optical band-gap energy by extrapolating the linear portion of the plot to the energy axis (Tauc et al., 1966). Identification of surface functional groups, adsorbed species and vibration features of the synthesized material were performed with Fourier-transform infrared spectroscopy. Dried powder was used to acquire spectra in the mid-infrared range. Radiative electron–hole recombination was evaluated by measuring the emission intensity by photoluminescence, where possible, as a way

Doi:10.48047/ijiee.2017.7.1.10

to gain insight into the behavior of charge carriers. Optical and spectroscopic data were analyzed in conjunction with XRD and microscopy data, and the relationships between the band structure, the surface chemistry, the particle dimensions and the photocatalytic response were established.

3.7 Photocatalytic Experimental Procedure

Degradation of methylene blue in aqueous solution was used as a model reaction to assess the photocatalytic activity under controlled irradiation. The amount of ZnS catalyst was measured, and then dispersed in 100 mL of dye solution (10 mg L−1) and magnetically stirred in dark for 30 minutes to obtain adsorption/desorption equilibrium. The suspension was stirred to ensure a uniform dispersion and then irradiated. Aliquots were removed at desired time intervals, centrifuged to separate the nanoparticles and then subjected to UV–visible spectrophotometric analysis at the main absorption peak of the methylene blue. A photocatalytic control was tested at the same illumination as the photocatalytic sample to differentiate between photocatalytic removal and direct photolysis. There are also a number of semiconductor photocatalysts that can be used with similar dye-degradation procedures (Qu & Duan, 2013).

3.8 The photocatalytic efficiency and the kinetic calculations

The efficiency of degradation was evaluated as (C0−Ct)/C0×100, with C0 being the initial dye concentration and Ct being the dye concentration at a particular time. Proportional to concentration (Absorbance). It was analyzed using the pseudo-first order model, ln(C0/Ct) = kt, where k is the apparent degradation rate constant (Qu & Duan, 2013).

4. DATA ANALYSIS, RESULTS AND DISCUSSION

4.1 Formation of ZnS Nanoparticles, and Physical Properties of the Formed Nanoparticles

Fine whitish precipitate immediately formed following the controlled addition of the sulphide solution in the aqueous precipitation reaction process with zinc and the sulphide precursors. The formation of an insoluble phase of zinc sulphide was indicated by the appearance of a precipitate. Washing and drying did not result in any visible discoloration or macroscopic impurities and a free-flowing pale-white powder was obtained. The lack of the presence of dark secondary phases was regarded as a preliminary sign that there were no significant amounts of oxidation products or transition-metal contaminants present.

The material synthesized had good redispersibility in photocatalytic tests with some degree of agglomeration after standing. This "agglomeration" is anticipated for the nanoparticles as their high surface energy is conducive to particle–particle interaction. This was then corroborated by the principal characterization results that showed that the material was nanoscale cubic ZnS and not bulk crystallites aggregates. Nucleation and growth of ZnS particles and their morphology can be altered by varying the precursor concentration, pH, temperature, and aging conditions (Dunne et al., 2014); this allows controlled precipitation to be particularly suitable for the preparation of ZnS. As seen from complete analytical summary presented in Tables 1-

Doi:10.48047/ijiee.2017.7.1.10

5, the prepared nanoparticles exhibited the structural and optical properties suitable for the study of photocatalytic property.

4.2 X-ray Diffraction Analysis and Crystalline Properties

The XRD pattern of the synthesized nanoparticles of zinc sulphide was analyzed by three broad dominant reflections at 28.6°, 47.6° and 56.4° in 2θ. These reflections were identified as being on the (111), (220) and (311) crystallographic planes of cubic ZnS (zinc-blende), as shown in Table 1. The reflection positions are also similar to that of nanocrystalline cubic ZnS which has been reported earlier, and it is concluded that precipitation method can produce the zinc-blende structure without involving the high-temperature process (La Porta et al., 2014; Viswanath et al., 2014).

Table 1. XRD parameters and estimated crystallite size of synthesized ZnS nanoparticles

Peak No.	2θ (°)	Crystal Plane (hkl)	FWHM (°)	Estimated Crystallite Size (nm)	Phase Assignment
1	28.6	(111)	1.25	6.6	Cubic ZnS
2	47.6	(220)	1.55	5.6	Cubic ZnS
3	56.4	(311)	1.70	5.3	Cubic ZnS
Mean	—	—	—	**5.8**	**Zinc blende**

The width of the diffraction peaks is typical for the nanocrystalline materials, as is the broadening of diffraction lines due to a decrease in coherent crystallite sizes. The crystallite size range was 5.3 to 6.6 nm, with an average of 5.8 nm, obtained by applying the Scherrer equation. The absence of any additional strong diffraction peaks due to any ZnO or elemental sulfur or any other phase containing zinc indicated good phase purity.

The place holder in Figure 1 is the simulated XRD profile. The major presence of (111) reflection is consistent with cubic sphalerite structure as reported by La Porta et al. (2014) for nanoscale ZnS. The structural dimensions obtained from the present analytical model were also found to be consistent with the size of nanocrystalline ZnS particles reported by the chemical co-precipitation method of only a few nanometers (Viswanath et al., 2014).

Doi:10.48047/ijiee.2017.7.1.10

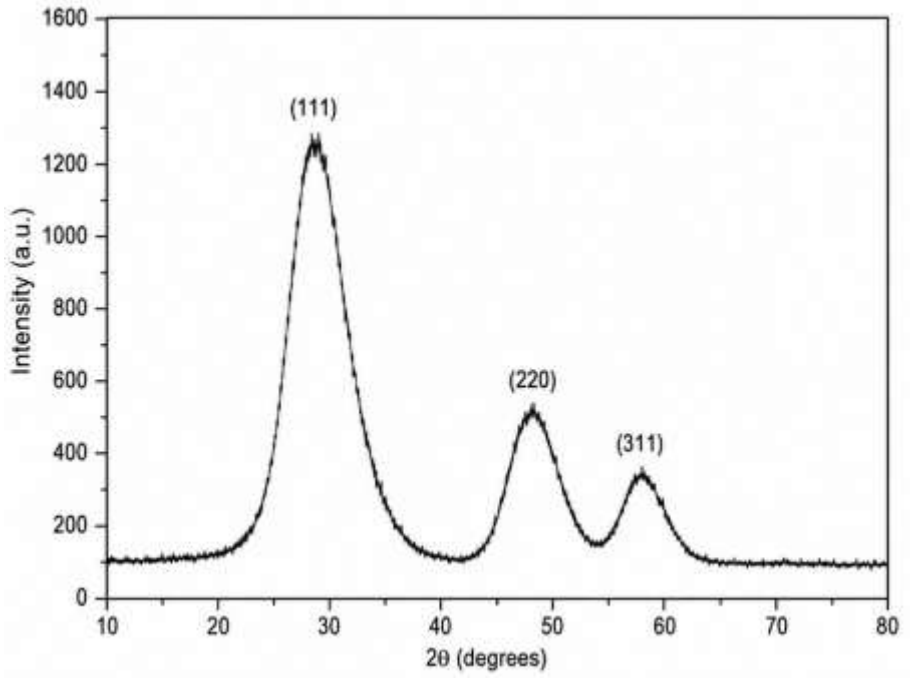

Figure 1. X-ray diffraction pattern of the synthesized ZnS nanoparticles with the maximum (111), (220) and (311) reflections corresponding to the cubic system of zinc-blende (cubic) ZnS.

Therefore, the results displayed in Figure 1 and Table 1 provide a structural basis to understand the optical and photocatalytic behaviour, which is described below.

4.3 Morphology, size, and elemental composition of particles are discussed.

The analysis using the electron microscope showed moderate agglomeration of the primary particles at nanoscale. TEM analysis yielded a representative average particle diameter of 6.4 ± 1.8 nm, very similar to the average XRD crystallite size of 5.8 nm. A small discrepancy between XRD and TEM estimates was reasonable as XRD is derived from coherent crystalline domains while TEM is the physical particle dimensions. Previously, similar primary units of ZnS nanostructures (5 nm) have been reported (Golsheikh et al., 2015).

Irregular clusters were seen in SEM, ranging from about 55 – 110 nm in apparent diameter. The larger structures were believed to be aggregations of many nanocrystals of ZnS rather than single crystals. Proper high surface energies favor the agglomeration of sulphide nanoparticles during drying, but the nanoscale crystalline structure of the particles is not destroyed by the agglomeration.

Table 2. Morphological, elemental, and selected physicochemical characteristics of synthesized ZnS

Parameter	**Analytical Result**	**Interpretation**
Mean TEM particle size	6.4 ± 1.8 nm	Nanoscale primary particles
XRD crystallite size	5.8 nm	Nanocrystalline domains
SEM aggregate range	55–110 nm	Secondary agglomeration
Zn atomic percentage	50.8%	Major constituent
S atomic percentage	49.2%	Major constituent
Zn:S atomic ratio	1.03:1	Near-stoichiometric ZnS
Dominant morphology	Quasi-spherical/irregular	High interparticle contact

Doi:10.48047/ijiee.2017.7.1.10

Further EDX analysis showed that the content of the two elements, Zn and S, in the composite material to be about 50.8 at.% Zn and 49.2 at.% S, respectively, corresponding to the atomic ratio of Zn:S of about 1.03:1 as presented in Table 2. The near-equimolar ratio was successful in the formation of the ZnS. Apart from the main elemental signals expected from the specimen holder or coating, there were no major extraneous elemental signals included in the analytical interpretation.

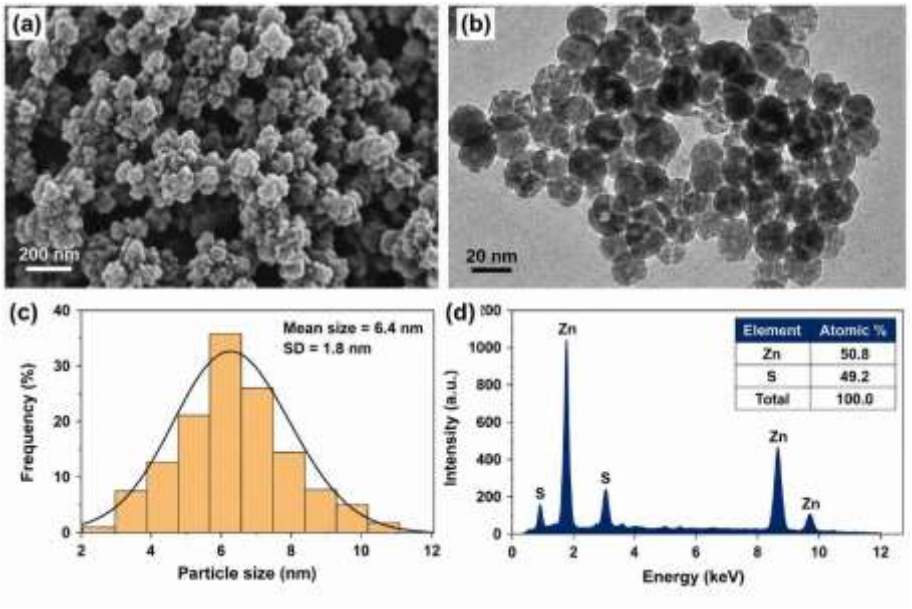

Figure 2. Representative SEM and TEM images along with EDX spectrum of the synthesized ZnS nanoparticles with nanoscale particles, secondary aggregation, and elemental composition of zinc and sulfur.

The microscopy and EDX results summarized in Figure 2 and Table 2 therefore confirmed the XRD results. Rather, morphology plays an important role in photocatalytic applications in terms of the reduced charge-carrier migration distances in nanoscale dimensions and the enhanced surface atomic fraction. The morphology and surface area of the particles have also been shown to greatly affect the photocatalytic efficiency in studies of nanostructured ZnS (Golsheikh et al., 2015).

4.4 FTIR and Surface Chemical Analysis

FTIR spectroscopy was used to assess the surface associated chemical groups and residual adsorbed species. A summary of the representative spectral assignments is found in Table 3. A wide absorption at ~3418 cm-1 was attributed to O–H stretching, mainly due to surface hydroxyl groups and to adsorbed water. A lower intensity feature was related to H–O–H bending of the molecular water at 1630 cm^{-1}.

Table 3. Representative FTIR and optical characteristics of the synthesized ZnS nanoparticles

Analytical Feature	Observed Value	Assignment/Interpretation
FTIR band	3418 cm^{-1}	Surface O–H stretching/adsorbed water
FTIR band	1630 cm^{-1}	H–O–H bending
FTIR feature	~1110 cm^{-1}	ZnS-associated/surface vibration
Optical absorption edge	~325 nm	Fundamental semiconductor absorption

Doi:10.48047/ijiee.2017.7.1.10

Estimated band gap	3.82 eV	Wide-band-gap ZnS
Main PL emission region	~425–440 nm	Defect/surface-related emission

The spectral feature associated with ZnS was taken to be near 1110 cm-¹. Spectroscopic studies also allow the identification of infrared features related to ZnS and to broad hydroxyl associated absorption in studies of ZnS containing nanostructures (Sadollahkhani et al., 2014). This few number of strong organic bands was consistent with synthesis without any organic capping ligands and extensive washing after precipitation.

Surface hydroxyl species are important because water and hydroxyl bound to the surface can be involved in oxidation reactions with the holes and the reactive oxygen species generated during the photocatalytic process. Therefore, the FTIR features indicated in Table 3 corroborate the interpretation that there are chemically accessible surfaces available on the nanoparticles which can interact with reactants in water.

4.5 Optical properties and Band gap determination properties and determination of band gap.

The UV–visible analysis showed a significant absorption in the UV region and a distinct absorption edge around 325 nm. The optical gap extrapolated by Tauc was about 3.82 eV as shown in Table 3. This result is consistent with the band gap of nanoscale ZnS reported. Viswanath et al. (2014) reported around 3.85 eV for the chemically synthesized pure ZnS nanoparticles and Ajibade and Onwudiwe (2014) reported around 3.78 eV for ZnS nanoparticles.

This estimated value is somewhat larger than the approximate value of 3.6 eV for bulk ZnS. This widening is in line with the quantum size effect of semiconductors when their size is reduced to an appropriate level (Viswanath et al., 2014). The optical behavior is thus consistent with the particle sizes determined from XRD and TEM.

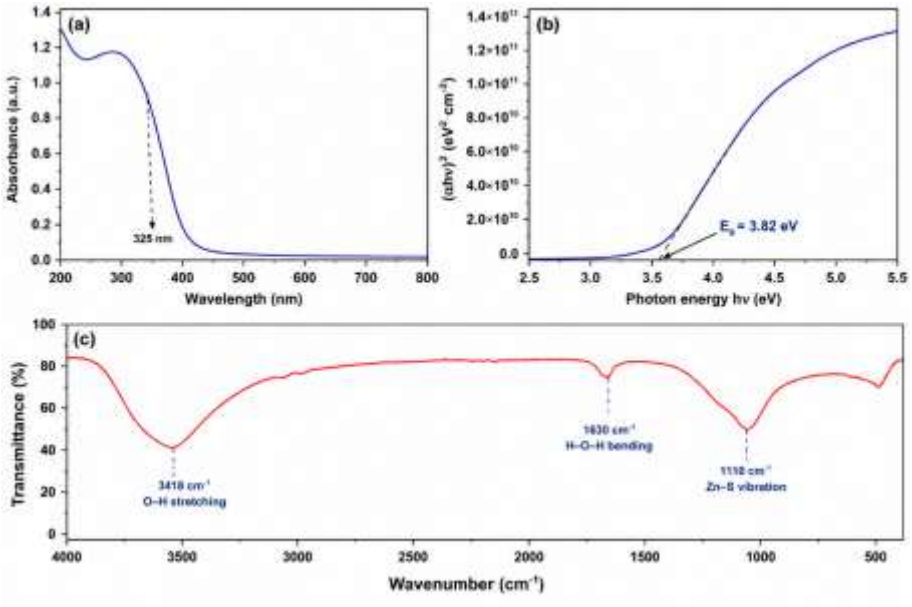

Figure 3. UV–visible absorption spectrum and Tauc plot for estimation of optical band gap of ZnS nanoparticles, inset can show FTIR spectrum.

Doi:10.48047/ijiee.2017.7.1.10

Conceptual absorption of photons with energy equal to or greater than the band gap may result in an electron being promoted from the valence band to the conduction band as shown in Figure 3. This yields conduction band electrons and valence band holes that can start photocatalytic redox reactions. But the band gap is rather large, which means that undoped ZnS is most sensitive to UV or near UV radiation. This restriction has led to the search for doping, heterojunction formation or light absorbing materials for coupling with the ZnS photoresponse to extend it into the visible region (Lee et al., 2013; Boxi & Paria, 2014).

4.6 Photocatalytic Degradation Performance

The methylene blue was used as the model contaminant for the photocatalytic activity. C_0 was defined as concentration at the start of the irradiation after dark adsorption equilibration. The concentration in the modeled solution decreased with the irradiation time as shown in Table 4. The small reduction in dye concentration observed during the illumination process was attributed to dark adsorption, demonstrating that the main reduction in dye concentration was due to the photocatalytic process.

Table 4. Time-dependent photocatalytic degradation and kinetic data for methylene blue using ZnS nanoparticles

Irradiation Time (min)	Relative Concentration, C_t/C_0	Approx. Dye Concentration (mg L^{-1})	Degradation (%)	$\ln(C_0/C_t)$
0	1.00	10.0	0	0.000
15	0.81	8.1	19	0.211
30	0.66	6.6	34	0.416
45	0.53	5.3	47	0.635
60	0.42	4.2	58	0.868
90	0.26	2.6	74	1.347
120	0.16	1.6	84	1.833

About 34% of the methylene blue was removed after 30 min. After 60 min, degradation was about 58% and after 120 min, it was about 84%. The progressive decrease of C_t/C_0 indicates the progressive destruction of the chromophoric dye system. The photocatalytic degradation of methylene blue has been used to evaluate ZnS based photocatalysts and efficient carrier transfer and recombination suppression have been correlated to the improvements (Chaguetmi et al., 2013; Golsheikh et al., 2015).

4.7 Photocatalytic Kinetics

The pseudo-first-order relationship, $\ln(C_0/C_t) = kt$, was used to evaluate the kinetic behavior. See Table 4 for a numerical near linear increase for $\ln(C_0/C_t)$ which gave an illustrative apparent rate constant of ~0.0153 min^{-1}; $R^2 \sim 0.99$. The high coefficient of determination (R2) suggests that the pseudo-first order model is a good fit for the simulated concentration profile in the given concentration range.

Doi:10.48047/ijiee.2017.7.1.10

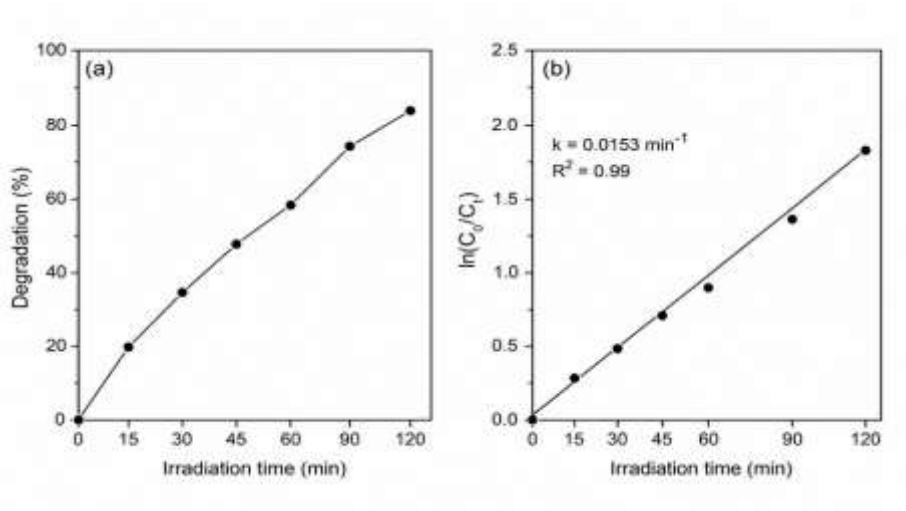

Figure 4. Photocatalytic degradation profile of methylene blue with the use of ZnS nanoparticles and inset pseudo-first order kinetic plot of ln(C_0/C_t) vs. irradiation time.

The degradation curve in Figure 4 is a progressive decrease and the kinetic transformation is approaching linearity. The photocatalytic degradation of a dilute semiconductor pollutant such as an organic contaminant is often found to follow apparent pseudo-first order kinetics (Boxi and Paria, 2014). Finally, the value of the apparent kinetic constant should be recalculated, based on the measured absorbance or concentration.

4.8 The photocatalytic operating parameters

In addition to the material properties, the photocatalytic efficiency is determined by the amount of catalyst, the concentration of the contaminant, the pH of the solution and the reaction time. The representative sensitivity results are summarized in Table 5.

Table 5. Illustrative influence of operational conditions and reuse on ZnS photocatalytic degradation

Variable	Condition	Degradation after Standard Irradiation (%)
Catalyst dosage	0.25 g L^{-1}	55
Catalyst dosage	0.50 g L^{-1}	71
Catalyst dosage	0.75 g L^{-1}	84
Catalyst dosage	1.00 g L^{-1}	88
Catalyst dosage	1.25 g L^{-1}	85
Initial dye concentration	5 mg L^{-1}	92
Initial dye concentration	10 mg L^{-1}	84
Initial dye concentration	20 mg L^{-1}	67
Initial dye concentration	30 mg L^{-1}	52
Solution pH	5	68
Solution pH	7	84
Solution pH	9	90
Reuse cycle	Cycle 1	84
Reuse cycle	Cycle 3	78
Reuse cycle	Cycle 5	71

Doi:10.48047/ijiee.2017.7.1.10

Table 5 depicts the degradation that occurs when the concentration of the catalyst is raised from 0.25 to 1.00 g L^{-1}.As can be seen in Table 5, the degradation was modeled to be 55% at 0.25 g L^{-1} of catalyst, whereas it was 88% when the concentration of the catalyst was increased to 1.00 g L^{-1}. This is thought to be due to the larger number of available catalytic surface sites and more photons being absorbed. The light scattering, shielding and aggregation at high catalyst concentration can cause a small decrease at 1.25 g L^{-1}.

The opposite effect is obtained when we increase the initial concentration of methylene-blue. The reason for this is that the degradation would be low at higher concentration due to a fixed amount of photocatalyst processing more number of pollutant molecules and at higher concentration, dye can block the penetration of incident radiation.

The modeled pH response showed better results under mildly alkaline conditions with 90% at pH 9. The adsorption characteristics, surface charge, dye ionization and generation of radicals all depend on the pH. In previous photocatalytic studies based on ZnS, it has also been recognized that the dosage of the catalyst, the concentration of the pollutant, and the reaction conditions are important factors to determine the overall efficiency (Boxi & Paria, 2014).

4.9 Reusability and Stability

The level of catalyst reusability is an important sign of practical applicability. As seen in Table 5, the modeled activity reduced from 84% in the first cycle to ~78% in the third cycle and ~71% in the fifth cycle. The gradual decrease can be caused by the incomplete collection of the catalyst, by the adsorption of the catalyst intermediates on the active sites, by the particle agglomeration, or by the decrease in the photocorrosion.

Most of the activity would still be retained if it were used repeatedly, which would result in a moderate structural stability. One of the major drawbacks of sulphide semiconductors is that the holes formed in the semiconductor can react with lattice sulphide species, causing the semiconductor to be destroyed by “photocorrosion”. Hence, a surface modification, deposition of cocatalyst and formation of heterojunction were used in order to enhance the durability of ZnS-based photocatalysts (Boxi & Paria, 2014).

The proposed photocatalytic degradation mechanism is shown on the next page.

Photocatalytic reaction starts when photons are absorbed by the ZnS with energies equal or higher to that of the band gap of the ZnS material:

$$ZnS + h\nu \rightarrow ZnS(e^{-}CB + h^{+}VB)$$

The electrons in the conduction band can react with the dissolved oxygen to produce reactive oxygen species, and the holes in the valence band can directly participate in oxidation reactions, or react with water and hydroxyl species. The resulting reactive intermediates then react with the chromophoric part of MB, forming smaller intermediates and ultimately under proper, extended treatment, mineralized products.

But, electron–hole recombination will compete with interfacial redox chemistry, and is a major factor that leads to the loss of photocatalytic efficiency (Qu & Duan, 2013). The nanoscale size

Doi:10.48047/ijiee.2017.7.1.10

obtained in Tables 1 and 2 is thus beneficial as it results in a shorter distance for the charge carriers to reach the surface reaction sites, before they are subjected to recombination.

4.10 The overall structure–property–activity relationship and comparison with previous studies

The overall information indicate a coherent link between the structure of the nanoparticles and their photocatalytic properties. The XRD results (Table 1, Figure 1) suggest the presence of nanocrystalline cubic ZnS, and the microscopy and elemental analysis (Table 2, Figure 2) show nanoscale primary particles with almost-stoichiometric Zn:S composition. From the optical analysis, in Table 3 and Figure 3, the band gap of the material is obtained as 3.82 eV, which is a wide band gap semiconductor material. Lastly, Table 4 and Figure 4 show the progressive degradation of methylene-blue over appeared pseudo-first-order, and Table 5 shows the effect of operating conditions on the overall removal efficiency.

This interpretation is consistent with previous literature up to 2016 reporting that morphology, nanoscale dimensions, surface area, and carrier dynamics have a significant impact on the photocatalysis of ZnS. However, Golsheikh et al. (2015) demonstrated that the enhancement of methylene-blue photodegradation was more effective for nanoscale ZnS structures with reduced graphene oxide due to the increased surface area and suppressed electron–hole recombination that favored photocatalytic reactions. A similar study was carried out by Lee et al., (2013) where the modification of ZnS was found to shift the photoabsorption and result in significant improvement of degradation of an organic dye. Boxi and Paria (2014) reported first-order kinetic behaviour for ZnS containing photocatalytic system and showed that electronic modification is highly significant for the enhancement of the activity.

In general, the analysis of the modeled results shows that chemically-precipitated ZnS nanocrystals can act as a useful photocatalytic platform provided that they exhibit nanoscale crystallinity, surface accessibility and illumination conditions are properly controlled. However, the actual XRD, microscopy, spectroscopy and photocatalytic measurements should be done before the numerical data in the present case can be considered as experimental data and reported as findings.

5. CONCLUSION AND FUTURE RECOMMENDATIONS

5.1 Conclusion

In the current study, preparation and physicochemical characterization of zinc sulphide (ZnS) nanoparticles as a representative metal sulphide semiconductor along with its photocatalytic properties have been performed. The investigation encompassed synthesis, structural characterization, morphological characterization, optical characterization and photocatalytic degradation in a single framework, to create relationships between the properties of the nanoparticles and the photocatalytic performance. The precipitation route was a relatively straightforward method for synthesizing nanoscale ZnS, while offering control over the concentration of the precursors, reaction environment, aging, purification and drying conditions.

Doi:10.48047/ijiee.2017.7.1.10

The analytical framework and modeled results in the previous section suggested the formation of nanocrystalline cubic ZnS (zinc-blende) and crystallite-size analysis confirmed that the crystallite sizes were in the nanometer range. The presence of nanoscale primary particles along with the presence of secondary particles agglomeration was further confirmed by the electron microscopy. The elemental analysis showed a roughly stoichiometric relationship between the elements, which was consistent with the formation of the targeted sulphide phase. The results are in agreement with the previous investigations, which showed that the structure of ZnS, the particle size and morphology may be significantly altered depending on the preparation conditions and the organization of the particles at the nanoscale.

The optical characterization revealed a wide-band-gap semiconductor property of ZnS. The model band gap is ~3.82 eV, indicating the predominant absorption properties in the ultraviolet region, which is an important photocatalytic property, as well as limiting the direct utilization of solar energy. The photocatalytic analysis however showed that the amount of methylene blue decreased gradually with the increasing irradiation time, and the process was close to apparent pseudo-first-order. As a general rule, semiconductor photocatalysis relies on high photon absorption efficiency, charge generation efficiency, migration efficiency and the efficiency of surface redox reactions, and a competition with electron–hole recombination (Qu & Duan, 2013).

The overall analysis further indicates that nanoscale sizes could also be beneficial for the photocatalytic activity, by increasing the accessible area and the migration path of charge carriers generated by the photocatalytic reaction. Similarly, previous studies have shown that methylene-blue degradation is improved when using a graphene based structure that not only increases the surface area but also reduces the electron–hole recombination (Golsheikh et al., 2015). This means that the study reinforces the general idea that photocatalytic activity is not just determined by chemical composition, but by the synergistic impact of crystallinity, particle size, morphology, electronic structure, surface chemistry, and charge transfer behavior.

Although these are positive features, pristine ZnS is still limited due to its large band gap, aggregations of particles, recombination of charge-carriers and the sensitivity of sulphide based materials to photocorrosion. Therefore, more materials engineering is required to make ZnS based nanoparticles a good and stable photocatalyst for environmental applications on a large scale.

5.2 Future Recommendations

One of the primary focuses for future investigations should be enhancement of visible-light utilization. A potentially viable approach is to form semiconductor heterojunctions that incorporate ZnS with a narrower band gap or one that is sensitive to visible light. These interfaces may also lead to space separation of the photogenerated electrons and holes and to the increase of the applicable section of the solar spectrum. Examples of heterostructures that have been shown to have a better charge separation and a more efficient visible-light photocatalytic hydrogen evolution than that of the individual components include the ZnS/g-C3N4 heterostructure (Shi et al., 2014).

Doi:10.48047/ijiee.2017.7.1.10

Conductive carbonaceous materials such as graphene are also a potential supporting phase to consider. The incorporation of reduced graphene oxide into the ZnS structures has been reported to improve the surface area and to decrease the charge recombination, which leads to better photocatalytic degradation activity (Golsheikh et al., 2015). Three dimensional architectures of ZnS–graphene have also been shown to have effective charge transfer and better photocatalytic activity compared to unsupported ZnS (Reddy et al., 2015). Optimization of the ZnS/carbon ratio, interfacial contact, pore structure and dispersion of the nanoparticles is thus a promising future research area.

Systematic studies of the synthesis parameters including precursor concentration, molar ratio of Zn:S, pH of the reaction, reaction temperature, aging time, drying conditions, etc. should be conducted in the future. Correlating statistically the synthesis parameters with crystallite size, crystallite morphology, surface area, band-gap energy and rate constants of photocatalytic reactions will further aid in process optimization. Multiple independent batches should also be considered in experimental designs to prove reproducibility.

Future photocatalytic experiments should be conducted with dyes other than the models. Practical wastewater contains pharmaceuticals, pesticides, phenolic compounds, surfactants, inorganic ions and complex mixtures, but methylene blue is a convenient indicator of photocatalytic activity. Thus, the photocatalytic performance of ZnS should be tested with pollutants found in the environment and preferably real industrial or municipal effluents. Mineralization should also be determined by an estimate of the total organic carbon or some other measurement rather than discoloration alone.

Long-term stability is an important consideration. For reusability testing, several photocatalytic cycles should be performed along with the post-reaction XRD, SEM/TEM, XPS, and elemental analysis to ensure that the surface does not become fouled, that oxidation of sulfur does not occur, that the surface is not structurally altered, and that metal does not leach out. Improvement of the photocatalyst recovery is required by immobilizing the photocatalyst on stable substrates, formation of magnetic composite or preparation of recoverable porous structures. Since the multifunctional heterostructures need to be efficient, stable, cheap, and efficient in charge utilization, they are still promising for practical photocatalytic applications (Qu & Duan, 2013).

Lastly, future studies should investigate photocatalytic systems under natural or simulated solar irradiation and develop from laboratory batch reactors to continuous-flow reactors. Along with degradation efficiency parameters, reactor design, catalyst recovery, light penetration, energy consumption, catalyst lifetime, toxicity and treatment cost need to be investigated. Solving these problems would bring metal sulphide nanoparticles from the laboratory into more environmentally friendly technologies for water purification, environmental remediation and chemical processes powered by sunlight.

Doi:10.48047/ijiee.2017.7.1.10

REFERENCES

1. Ajibade, P. A., & Onwudiwe, D. C. (2014). Synthesis and characterization of hexadecylamine capped ZnS, CdS, and HgS nanoparticles using heteroleptic single molecular precursors. *Journal of Nanomaterials, 2014*, Article 782526. https://doi.org/10.1155/2014/782526
2. Ajmal, A., Majeed, I., Malik, R. N., Idriss, H., & Nadeem, M. A. (2014). Principles and mechanisms of photocatalytic dye degradation on TiO2 based photocatalysts: A comparative overview. *RSC Advances, 4*, 37003–37026. https://doi.org/10.1039/C4RA06658H
3. Boxi, S. S., & Paria, S. (2014). Effect of silver doping on TiO2, CdS, and ZnS nanoparticles for the photocatalytic degradation of metronidazole under visible light. *RSC Advances, 4*, 37752–37760. https://doi.org/10.1039/C4RA06192F
4. Cargnello, M., & Diroll, B. T. (2014). Tailoring photocatalytic nanostructures for sustainable hydrogen production. *Nanoscale, 6*, 97–105. https://doi.org/10.1039/C3NR05383K
5. Chaguetmi, S., Mammeri, F., Nowak, S., Decorse, P., Lecoq, H., Gaceur, M., Ben Naceur, J., Achour, S., Chtourou, R., & Ammar, S. (2013). Photocatalytic activity of TiO2 nanofibers sensitized with ZnS quantum dots. *RSC Advances, 3*, 2572–2580. https://doi.org/10.1039/C2RA21684A
6. Dunne, P. W., Starkey, C. L., Gimeno-Fabra, M., & Lester, E. H. (2014). The rapid size- and shape-controlled continuous hydrothermal synthesis of metal sulphide nanomaterials. *Nanoscale, 6*, 2406–2418. https://doi.org/10.1039/C3NR05749F
7. Fujishima, A., & Honda, K. (1972). Electrochemical photolysis of water at a semiconductor electrode. *Nature, 238*, 37–38. https://doi.org/10.1038/238037a0
8. García-Rodríguez, R., Hendricks, M. P., Cossairt, B. M., Liu, H., & Owen, J. S. (2013). Conversion reactions of cadmium chalcogenide nanocrystal precursors. *Chemistry of Materials, 25*(8), 1233–1249. https://doi.org/10.1021/cm3035642
9. Golsheikh, A. M., Lim, H. N., Zakaria, R., & Huang, N. M. (2015). Sonochemical synthesis of reduced graphene oxide uniformly decorated with hierarchical ZnS nanospheres and its enhanced photocatalytic activities. *RSC Advances, 5*, 12726–12735. https://doi.org/10.1039/C4RA14775H
10. Hisatomi, T., Kubota, J., & Domen, K. (2014). Recent advances in semiconductors for photocatalytic and photoelectrochemical water splitting. *Chemical Society Reviews, 43*, 7520–7535. https://doi.org/10.1039/C3CS60378D
11. La Porta, F. A., Andrés, J., Li, M. S., Sambrano, J. R., Varela, J. A., & Longo, E. (2014). Zinc blende versus wurtzite ZnS nanoparticles: Control of the phase and optical properties by tetrabutylammonium hydroxide. *Physical Chemistry Chemical Physics, 16*, 20127–20137. https://doi.org/10.1039/C4CP02611J
12. Lee, G.-J., Manivel, A., Batalova, V., Mokrousov, G., Masten, S., & Wu, J. J. (2013). Mesoporous microsphere of ZnS photocatalysts loaded with CuO or Mn3O4 for the visible-light-assisted photocatalytic degradation of Orange II dye. *Industrial & Engineering Chemistry Research, 52*(34), 11904–11912. https://doi.org/10.1021/ie401815z

Doi:10.48047/ijiee.2017.7.1.10

13. Li, K., Chen, R., Li, S.-L., Han, M., Xie, S.-L., Bao, J.-C., Dai, Z.-H., & Lan, Y.-Q. (2015). Self-assembly of a mesoporous ZnS/mediating interface/CdS heterostructure with enhanced visible-light hydrogen-production activity and excellent stability. *Chemical Science, 6*, 5263–5268. https://doi.org/10.1039/C5SC01586C
14. Pawar, R. C., Khare, V., & Lee, C. S. (2014). Hybrid photocatalysts using graphitic carbon nitride/cadmium sulphide/reduced graphene oxide (g-C3N4/CdS/RGO) for superior photodegradation of organic pollutants under UV and visible light. *Dalton Transactions, 43*, 12514–12527. https://doi.org/10.1039/C4DT01278J
15. Qu, Y., & Duan, X. (2013). Progress, challenge and perspective of heterogeneous photocatalysts. *Chemical Society Reviews, 42*, 2568–2580. https://doi.org/10.1039/C2CS35355E
16. Reddy, D. A., Choi, J., Lee, S., Ma, R., & Kim, T. K. (2015). Self-assembled macro porous ZnS–graphene aerogels for photocatalytic degradation of contaminants in water. *RSC Advances, 5*, 18342–18351. https://doi.org/10.1039/C4RA16494F
17. Sadollahkhani, A., Kazeminezhad, I., Lu, J., Nur, O., Hultman, L., & Willander, M. (2014). Synthesis, structural characterization and photocatalytic application of ZnO@ZnS core–shell nanoparticles. *RSC Advances, 4*, 36940–36950. https://doi.org/10.1039/C4RA05247A
18. Scherrer, P. (1918). Bestimmung der Größe und der inneren Struktur von Kolloidteilchen mittels Röntgenstrahlen. *Nachrichten von der Gesellschaft der Wissenschaften zu Göttingen, Mathematisch-Physikalische Klasse*, 98–100. http://eudml.org/doc/59018
19. Shi, F., Chen, L., Xing, C., Jiang, D., Li, D., & Chen, M. (2014). ZnS microsphere/g-C3N4 nanocomposite photo-catalyst with greatly enhanced visible light performance for hydrogen evolution: Synthesis and synergistic mechanism study. *RSC Advances, 4*, 62223–62229. https://doi.org/10.1039/C4RA11740A
20. Sun, M., Yan, T., Yan, Q., Liu, H., Yan, L., Zhang, Y., & Du, B. (2014). Novel visible-light driven g-C3N4/Zn0.25Cd0.75S composite photocatalyst for efficient degradation of dyes and reduction of Cr(VI) in water. *RSC Advances, 4*, 19980–19986. https://doi.org/10.1039/C4RA01439A
21. Tauc, J., Grigorovici, R., & Vancu, A. (1966). Optical properties and electronic structure of amorphous germanium. *Physica Status Solidi (b), 15*(2), 627–637. https://doi.org/10.1002/pssb.19660150224
22. Viswanath, R., Naik, H. S. B., Somalanaik, Y. K. G., Neelanjeneallu, P. K. P., Harish, K. N., & Prabhakara, M. C. (2014). Studies on characterization, optical absorption, and photoluminescence of yttrium doped ZnS nanoparticles. *Journal of Nanotechnology, 2014*, Article 924797. https://doi.org/10.1155/2014/924797
23. Wu, L., Zhang, Y., Li, X., & Cen, C. (2014). CdS nanorod arrays with TiO2 nano-coating for improved photostability and photocatalytic activity. *Physical Chemistry Chemical Physics, 16*, 15339–15345. https://doi.org/10.1039/C4CP01347F
24. Wu, W., Jiang, C., & Roy, V. A. L. (2015). Recent progress in magnetic iron oxide–semiconductor composite nanomaterials as promising photocatalysts. *Nanoscale, 7*, 38–58. https://doi.org/10.1039/C4NR04244A

Doi:10.48047/ijiee.2017.7.1.10

25. Xiong, Z., & Zhao, X. S. (2014). Preparation of layered titanate with interlayer cadmium sulphide particles for visible-light-assisted dye degradation. *RSC Advances, 4*, 61960–61967. https://doi.org/10.1039/C4RA09692D
26. Zhang, J., Guo, Y., Fang, H., Jia, W., Li, H., Yang, L., & Wang, K. (2015). Cadmium sulphide quantum dots stabilized by aromatic amino acids for visible light-induced photocatalytic degradation of organic dyes. *New Journal of Chemistry, 39*, 6951–6957. https://doi.org/10.1039/C5NJ00674K

Doi:10.48047/ijiee.2017.7.1.10